REPORT DOCUMENTATION PAGE

Form Approved OMB NO. 0704-0188

1. REPORT DATE (DD-MM-YYYY)	2. REPORT TYPE	3. DATES COVERED (From - To)
	Technical Report	-

4. TITLE AND SUBTITLE
Nanoscale Imaging with a Single Quantum Dot

5a. CONTRACT NUMBER
W911NF-10-1-0310

5b. GRANT NUMBER

5c. PROGRAM ELEMENT NUMBER
0D10BG

6. AUTHORS
Chad Ropp, , Zachary Cummins, , Sanghee Nah, , John T. Fourkas, , Benjamin Shapiro2, , Edo Waks

5d. PROJECT NUMBER

5e. TASK NUMBER

5f. WORK UNIT NUMBER

7. PERFORMING ORGANIZATION NAMES AND ADDRESSES
University of Maryland - College Park
Office of Research Admin
University of Maryland
College Park, MD 27425 -141

8. PERFORMING ORGANIZATION REPORT NUMBER

9. SPONSORING/MONITORING AGENCY NAME(S) AND ADDRESS(ES)
U.S. Army Research Office
P.O. Box 12211
Research Triangle Park, NC 27709-2211

10. SPONSOR/MONITOR'S ACRONYM(S)
ARO

11. SPONSOR/MONITOR'S REPORT NUMBER(S)
58315-MS-DRP.1

12. DISTRIBUTION AVAILIBILITY STATEMENT
Approved for public release; distribution is unlimited.

13. SUPPLEMENTARY NOTES
The views, opinions and/or findings contained in this report are those of the author(s) and should not contrued as an official Department of the Army position, policy or decision, unless so designated by other documentation.

14. ABSTRACT
The ability to optically image with nanometer resolution is essential for understanding the electromagnetic properties of nanoscopic objects. The most common methods for performing nanoscale imaging are based on near-field scanning optical microscopy, which utilizes a tapered probe that can add unwanted distortion to images. Such distortion can be eliminated by probing with an isolated, point-like emitter. Here we present a method for performing nanoscale imaging using a deterministically positioned single quantum dot (QD). The QD is

15. SUBJECT TERMS
Near field imaging, plasmonics, quantum dot

16. SECURITY CLASSIFICATION OF:			17. LIMITATION OF ABSTRACT	15. NUMBER OF PAGES	19a. NAME OF RESPONSIBLE PERSON
a. REPORT	b. ABSTRACT	c. THIS PAGE			Edo Waks
UU	UU	UU	UU		19b. TELEPHONE NUMBER 301-405-5022

Report Title

Nanoscale Imaging with a Single Quantum Dot

ABSTRACT

The ability to optically image with nanometer resolution is essential for understanding the electromagnetic properties of nanoscopic objects. The most common methods for performing nanoscale imaging are based on near-field scanning optical microscopy, which utilizes a tapered probe that can add unwanted distortion to images. Such distortion can be eliminated by probing with an isolated, point-like emitter. Here we present a method for performing nanoscale imaging using a deterministically positioned single quantum dot (QD). The QD is manipulated to nanoscale precision by microfluidic flow control, which does not require the use of macroscopic manipulators. We use this technique to image the surface plasmon polariton (SPP) mode of a silver nanowire with resolution as fine as 10 nm by monitoring the coupling efficiency into the wire mode. The measured field distribution reveals nanoscale features such as localized modes at the wire ends and interference in the propagating SPP waves.

Nanoscale Imaging with a Single Quantum Dot

Chad Ropp[1], Zachary Cummins[2], Sanghee Nah[3], John T. Fourkas[3,4], Benjamin Shapiro[2], Edo Waks[1,5]

[1]*Department of Electrical and Computer Engineering and Institute for Research in Electronics and Applied Physics*

[2]*Fischell Department of Bio-Engineering and the Institute for Systems Research*

[3]*Department of Chemistry and Biochemistry*

[4]*Institute for Physical Science and Technology*

[5]*Joint Quantum Institute, National Institute of Standards and Technology*

University of Maryland, College Park, Maryland 20742, USA

The ability to optically image with nanometer resolution is essential for understanding the electromagnetic properties of nanoscopic objects[1-3]. The most common methods for performing nanoscale imaging are based on near-field scanning optical microscopy[4-8], which utilizes a tapered probe that can add unwanted distortion to images[9,10]. Such distortion can be eliminated by probing with an isolated, point-like emitter. Here we present a method for performing nanoscale imaging using a deterministically positioned single quantum dot (QD). The QD is manipulated to nanoscale precision by microfluidic flow control[11-13], which does not require the use of macroscopic manipulators. We use this technique to image the surface plasmon polariton (SPP) mode of a silver nanowire with resolution as fine as 10 nm by monitoring the coupling efficiency into the wire mode. The measured field distribution reveals nanoscale features such as localized modes at the wire ends and interference in the propagating SPP waves.

Imaging with a nanoscopic probe presents significant challenges due to the lack of suitable techniques for nanoscale particle manipulation. The most common methods for

particle manipulation are based on optical tweezers[14], but optical gradient forces scale with particle volume, making the manipulation of nanoscopic objects challenging[15]. Methods for incorporating nanoparticle emitters on tapered-fiber scanning microprobe tips have been demonstrated, but currently these techniques have been limited to an imaging resolution of about 100 nm[8]. Techniques based on mechanical placement of diamond nanocrystals along a surface have achieved nanoscale positioning accuracy[16,17], but so far have only provided sparse sampling of the electromagnetic mode with too few data points to reconstruct an accurate image. Random diffusion has also been used to decorate plasmonic hot spots with single molecular emitters, achieving imaging resolution as fine as 1.2 nm[18]. However, this procedure is entirely stochastic and cannot be used to probe a desired location or target on demand.

In this work we demonstrate a method for imaging with nanometer resolution using a single quantum dot (QD) by utilizing the enhanced electromagnetic interactions between the QD and the surface plasmon polariton (SPP) mode of a silver nanowire (AgNW). QDs are bright and robust nanoscale emitters, and are therefore ideal candidates for probing electromagnetic interactions. We use colloidally suspended CdSe QDs that are manipulated in a microfluidic device by controlling the flow of the surrounding liquid, enabling us to position a single QD near the AgNW with nanometric accuracy[12]. When a QD is positioned near the AgNW, energy from the photoexcited QD is non-radiatively transferred to the wire's SPP mode through an electric dipole interaction[19]. The efficiency of this process scales as the spontaneous emission rate of the QD into the SPP mode, which takes on the form $\Gamma_{SP} = \Gamma_0 \left|\mathbf{E}(\mathbf{r})\right|^2 / \left|\mathbf{E}_{\max}\right|^2$, where $\left|\mathbf{E}(\mathbf{r})\right|^2$ is the electromagnetic field intensity of the SPP mode, $\left|\mathbf{E}_{\max}\right|^2$ is the maximum electric field intensity of the mode, and Γ_0 is the spontaneous emission rate at the field maximum[20]. The electromagnetic mode profile of the SPP mode can therefore be determined by measuring the rate at which photons couple into the AgNW, which is monitored by observing the scattered light intensity from the wire end[19].

An optical image of the microfluidic device used to position QDs is shown in Fig. 1a. Four tapered microfluidic channels intersect at the control region where QD manipulation occurs (the dashed circle). AgNWs with an average diameter of 100 nm and an average length of 4 μm (SEM image in Fig. 1c inset) are deposited on the polydimethylsiloxane (PDMS) surface of the control region. The channels are filled with fluid containing QDs that become confined to a thin sheath along the surface due to the fluid chemistry[13]. Within this sheath, QDs are manipulated to nanometric precision using electroosmosis with feedback control[12,13]. The AgNW acts as an obstacle for the QDs, indicating that they are constrained to lie within 100 nm of the surface (the height of the AgNW). The device is mounted on an inverted microscope and QDs are imaged using a CCD camera. Their positions are tracked with sub-wavelength precision by fitting the diffraction spot to a Gaussian point spread function. The vision accuracy of the QD tracking algorithm was determined to be 9 nm by tracking an immobilized QD on a glass surface (see Supplementary Information). Details of the fluid composition, experimental setup, and nanowire synthesis are provided in the Methods section.

Fig. 1b. illustrates how imaging of an AgNW is performed. Within the control region, a single QD is selected and driven along a trajectory that samples the local field of the wire at a desired set of locations. The accuracy within which QDs can be positioned is measured to be 41 nm, ensuring that we can deterministically probe the wire mode at a desired location on-demand. The QD trajectory is selected to maximize data sampling near the wire surface (see Supplementary Information for both measurement of the QD positioning accuracy and selection of the QD trajectory). Figs. 1c-e are a series of images of a single QD being moved progressively closer to an AgNW. When the QD is in close proximity to the wire, light scatter is observed from the wire ends (Fig. 1e). A collection of such images can be used to map the SPP mode

of the AgNW by monitoring the scattered intensity at the ends of the nanowire as a function of the QD position.

Intensity variations due to QD blinking as well as local field modification of the pump by the AgNW can complicate interpretation of the scattered intensity. We account for these effects by normalizing the intensity scattered from the wire end by the intensity of the direct QD emission. The QD emission and the AgNW scatter are measured by summing the pixels within their respective windows (Fig. 1c-e). We define the normalized coupled intensity $\bar{I}$ as:

$$\bar{I}(x,y) = \frac{\sum_{n,m}\left(I_{n,m}^{NW} - I^{BKG}\right)}{\sum_{p,q}\left(I_{p,q}^{QD} - I^{BKG}\right)} \qquad (1)$$

where $I_{n,m}^{NW}$ and $I_{p,q}^{QD}$ are the intensities of the (n,m)th and (p,q)th pixels within the AgNW and QD windows respectively, while I^{BKG} is the average pixel background intensity. The background level is calculated by averaging pixels sufficiently far away from the AgNW and QD. The quantity $\bar{I}$ is directly proportional to the electromagnetic field intensity of the SPP mode.

Fig. 2a is a scatter plot of $\bar{I}$ as a function of QD position when the QD is near the midpoint of the AgNW (video provided in Supplementary Information). The shaded region represents the wire location as estimated from light scattered from the wire ends and an assumed AgNW radius of 50 nm. The color of each data point corresponds to $\bar{I}$ at that location, which is observed to increase as the QD approaches the AgNW. When the QD is closest to the wire, a maximal $\bar{I}$ of 0.12 is observed. Fig. 2b shows $\bar{I}$ as a function of radial distance from the wire axis. For a cylindrically symmetric AgNW, the evanescent field from the surface follows a Bessel function decay[21]. A fitting function $\left|\beta K_0(\alpha\rho)\right|^2$ is therefore used, where $K_0(\alpha\rho)$ is the zeroth-order modified Bessel

function, ρ is the radial distance from the AgNW axis, and α and β are fitting parameters (calculated to be 0.01 nm^{-1} and 0.51, respectively). The solid blue line in Fig. 2b is the Bessel-function fit and the red dashed line corresponds to the AgNW evanescent field as calculated using finite-difference time-domain (FDTD) simulation (see Methods). The FDTD solution is multiplied by a normalization constant to provide the best fit to the data. To determine the spatial accuracy of the measured positions, we calculate the root mean-squared distance of the measured results from the Bessel function fit (See Supplement), which is determined to be 10 nm. This estimate provides an upper bound on the spatial accuracy by making the worst-case assumption that all noise is due exclusively to fluctuations in the measured position. The estimated spatial accuracy is consistent with the 9 nm vision accuracy calculated previously.

Fig. 3a is a scatter plot of data recorded when a QD was scanned near one end of the AgNW while the intensity was monitored at the opposite end. Probing the AgNW tip required several minutes of QD scanning, over which sample drift becomes important. We corrected for the sample drift by calculating the QD position relative to the wire end that is tracked throughout the experiment by the same method that monitors the QD position. The ability to correct for drift represents an important practical advantage of this approach, enabling us to acquire images over long acquisition times without image distortion. As shown in Fig. 3a, enhanced coupling is observed near the end of the AgNW, which is attributed to a localized mode at the tip[19,22]. A maximal $\bar{I}$ of 0.34 is observed, which is significantly higher than the coupling measured at the middle of the wire. Data points located within the shaded wire region are attributed to the QD being pushed slightly on top of the wire, which does not act as a perfect obstacle.

The raw data presented in Fig. 3a can be used to construct an image of the field profile of the localized mode. The value of each pixel in the image is found by taking a

Gaussian-weighted average of the raw data. The Gaussian is centered at the location of the pixel and the standard deviation is set to 22 nm, corresponding to the root-mean-square combined spatial accuracy of the QD (10 nm) and the tracked AgNW end (20 nm) (see Supplementary Information). The additional error incurred by tracking the wire end is not fundamental to the imaging procedure and could be largely removed by using brighter tracking objects to monitor the drift. The resulting two-dimensional field profile is shown in Fig. 3b. Comparison of the measured field profile with the calculated mode profile attained from FDTD simulations shows good agreement between experiment and prediction (Fig. 3c).

In addition to the highly localized mode at the wire end, Figs. 3b and 3c suggest the presence of an oscillatory mode structure along the sides of the wire. To examine this mode structure in more detail, we probed the field along a 1 μm long region at one end of a wire. The measurement results are shown in Fig. 4a, where position is once again plotted relative to the wire end. In this measurement we used flow to position a QD as close as possible to the wire surface. Under these conditions most of the QD positions were measured within the shaded region. These data points are again attributed to being on top of the wire, where we measured $\bar{I}$ values as high as 0.16 (which is slightly larger than the values found in Fig. 2a). This increased coupling indicates that the QD is close to the AgNW surface.

A clear periodic pattern is observed in the scatter plot as the QD is moved along the length of the AgNW. These oscillatory fringes arise from interference between the QD emission propagating in the forward direction and reflected from the wire end[1]. The oscillatory pattern is more readily observed in the Gaussian image reconstruction in Fig. 4b. Fig. 4c. displays the calculated FDTD field intensity along the side of the AgNW, and exhibits good qualitative agreement with the measured data. In Fig. 4d, we plot $\bar{I}$ for data points within the shaded region in Fig. 4a and a sinusoidal fit. From the fit we

determine wavelength of the propagating SPP mode to be 368 nm. This value is slightly different than the 329 nm calculated with FDTD. This difference is likely due to use of parameters for bulk silver[23] in the simulation. Our AgNWs are bicrystalline[24] and are therefore expected to have a different dielectric constant than bulk silver, resulting in a different propagation constant.

In conclusion, we have demonstrated a method for imaging the field profile of surface plasmon polariton modes with nanometric resolution using enhanced atom-light interactions with an isolated single QD. The demonstrated approach provides a direct measurement of the electromagnetic field profile, and also enables deterministic control of these interactions by precise placement of the QD at different field locations. Fluid-based methods for three-dimensional tracking and control[25] of particles could also be incorporated to perform three-dimensional imaging with nanoscale accuracy. In addition, by combining this technique with methods for selective immobilization of QDs[13], our results can be extended from probing to a deterministic assembly of active quantum emitters and plasmonic structures for development of new nanoelectronic devices[26] and quantum optical circuits[27].

METHODS

Fluid composition. The control fluid is composed of 47.5% by volume ethoxylated-15 trimethylolpropane triacrylate resin (SR-9035, Sartomer)[28], 1.25 wt% rheology modifier (Acrysol RM-825, Rohm and Haas Co.)[29], 0.15% of a zwitterionic betaine surfactant[30], and CdSe/ZnS core-shell QDs (Ocean NanoTech©, Carboxylic Acid, 620 nm) in deionized water. The triacrylate resin causes the fluid sheath to form. The surfactant is introduced to improve EOF actuation on the PDMS surface while the rheology modifier is used to reduce Brownian motion and inhibit unwanted adhesion of the QDs to surfaces.

Experimental setup. The microfluidic device is composed of a molded PDMS cross pattern placed on top of a glass coverslip. The resulting channel is 5 μm in height with a control region that is approximately 100 μm in diameter. The QDs are excited by a highly defocused 532 nm light source with illumination intensity of 200 W/cm^2, and imaged onto an EMCCD camera (Hamamatsu C9100-13) operating at 20 Hz frame rate.

Synthesis of silver nanowires. Silver nanowires were synthesized by reducing $AgNO_3$ with ethylene glycol (EG)[24]. In a typical synthesis, 5 mL of EG (Fisher Scientific) was placed in a 50 mL round-bottom flask equipped with a condenser, a thermometer and a magnetic stirring bar. After the EG was heated to 160 °C in an oil bath, 0.5 mL of $PtCl_2$ (Aldrich, 1.5×10^{-4} M in EG) was injected into the solution to synthesize 1 - 5 nm precursor nanoparticles. After 4 min, 2.5 mL of $AgNO_3$ (Aldrich, 0.12 M in EG) and 5 mL of poly(vinyl pyrrolidone), (PVP, Mw ≈ 40,000, City Chemical LLC, 0.36 M in EG) were added simultaneously over 6 min with an accompanying color change from yellow to yellowish gray. When the $AgNO_3$ had been completely reduced by EG for 60 min, the solution was cooled to room temperature. To remove the remaining EG, PVP and silver nanoparticles, the solution was diluted with ethanol and centrifuged at 2000 rpm for 15 min. After repeating several times until the supernatant became transparent, the solution was redispersed in H_2O. The resulting bicrystalline[24] silver nanowires are 100 to 200 nm in diameter and 3 to 10 μm in length, as determined by scanning electron microscopy.

Finite different time domain simulation. Simulations were performed using the Lumerical FDTD Solutions software package (http://www.lumerical.com). A 4 μm long silver nanowire with 100 nm diameter was simulated surrounded by a background index of 1.4, which corresponds to the index of refraction for PDMS. The QD fluid was assumed to have the same index. The actual index of the fluid lies somewhere between water (1.3) and the index of the resin (1.47).

1. Ditlbacher, H. et al. Silver Nanowires as Surface Plasmon Resonators. *Phys. Rev. Lett.* **95**, 257403 (2005).

2. Imura, K. & Okamoto, H. Reciprocity in scanning near-field optical microscopy: illumination and collection modes of transmission measurements. *Opt. Lett.* **31**, 1474-1476 (2006).

3. Okamoto, K. et al. Near-field scanning optical microscopy of photonic crystal nanocavities. *Appl. Phys. Lett.* **82**, 1676 (2003).

4. Bozhevolnyi, S.I. & Vohnsen, B. Near-field optics with uncoated fiber tips: light confinement and spatial resolution. *J. Opt. Soc. Am. B* **14**, 1656-1663 (1997).

5. Hecht, B. et al. Scanning near-field optical microscopy with aperture probes: Fundamentals and applications. *J. Chem. Phys.* **112**, 7761 (2000).

6. Inouye, Y. & Kawata, S. Near-field scanning optical microscope with a metallic probe tip. *Opt. Lett.* **19**, 159-161 (1994).

7. Zenhausern, F., O'Boyle, M.P. & Wickramasinghe, H.K. Apertureless near-field optical microscope. *Appl. Phys. Lett.* **65**, 1623 (1994).

8. Cuche, A. et al. Near-field optical microscopy with a nanodiamond-based single-photon tip. *Opt. Express* **17**, 19969-19980 (2009).

9. Yao, H., Li, Z. & Gong, Q. Coupling-induced excitation of a forbidden surface plasmon mode of a gold nanorod. *Sci. China Ser. G-Phys. Mech. Astron.* **52**, 1129-1138 (2009).

10. Drezet, A., Cuche, A. & Huant, S. Near-field microscopy with a single-photon point-like emitter: Resolution versus the aperture tip? *Optics Communications* **284**, 1444-1450 (2011).

11. Armani, M., Chaudhary, S., Probst, R. & Shapiro, B. Using feedback control and micro-fluidics to steer individual particles. *18th IEEE Int. Conf. Micro Electro Mechan. Syst., Miami, FL* 855-858 (2005).doi:10.1109/MEMSYS.2005.1454064

12. Ropp, C. et al. Manipulating Quantum Dots to Nanometer Precision by Control of Flow. *Nano Letters* **10**, 2525-2530 (2010).

13. Ropp, C. et al. Positioning and Immobilization of Individual Quantum Dots with Nanoscale Precision. *Nano Letters* **10**, 4673-4679 (2010).

14. Ashkin, A., Dziedzic, J.M., Bjorkholm, J.E. & Chu, S. Observation of a single-beam gradient force optical trap for dielectric particles. *Opt. Lett.* **11**, 288-290 (1986).

15. Dienerowitz, M., Mazilu, M. & Dholakia, K. Optical manipulation of nanoparticles: a review. *J. Nanophoton.* **2**, 021875 (2008).

16. Huck, A., Kumar, S., Shakoor, A. & Andersen, U.L. Controlled Coupling of a Single Nitrogen-Vacancy Center to a Silver Nanowire. *Phys. Rev. Lett.* **106**, 096801 (2011).

17. Schell, A.W. et al. Single defect centers in diamond nanocrystals as quantum probes for plasmonic nanostructures. *Opt. Express* **19**, 7914-7920 (2011).

18. Cang, H. et al. Probing the electromagnetic field of a 15-nanometre hotspot by single molecule imaging. *Nature* **469**, 385-388 (2011).

19. Akimov, A.V. et al. Generation of single optical plasmons in metallic nanowires coupled to quantum dots. *Nature* **450**, 402-406 (2007).

20. Waks, E. & Sridharan, D. Cavity QED treatment of interactions between a metal nanoparticle and a dipole emitter. *Phys. Rev. A* **82**, (2010).

21. Balanis, C.A. *Advanced Engineering and Electromagnetics*. (John Wiley & Sons: 2011).

22. Laroche, T. & Girard, C. Near-field optical properties of single plasmonic nanowires. *Appl. Phys. Lett.* **89**, 233119 (2006).

23. Palik, E. *Handbook of optical constants of solids*. (Academic Press: Orlando, 1985).

24. Sun, Y., Yin, Y., Mayers, B.T., Herricks, T. & Xia, Y. Uniform Silver Nanowires Synthesis by Reducing AgNO3 with Ethylene Glycol in the Presence of Seeds and Poly(Vinyl Pyrrolidone). *Chemistry of Materials* **14**, 4736-4745 (2002).

25. Probst, R. & Shapiro, B. Three-dimensional electrokinetic tweezing: device design, modeling, and control algorithms. *J. Micromech. Microeng.* **21**, 027004 (2011).

26. Engheta, N. Circuits with Light at Nanoscales: Optical Nanocircuits Inspired by Metamaterials. *Science* **317**, 1698-1702 (2007).

27. Chang, D.E., Sorensen, A.S., Demler, E.A. & Lukin, M.D. A single-photon transistor using nanoscale surface plasmons. *Nat Phys* **3**, 807-812 (2007).

28. Liu, J., Gao, D., Li, H.-F. & Lin, J.-M. Controlled photopolymerization of hydrogel microstructures inside microchannels for bioassays. *Lab. Chip* **9**, 1301-1305 (2009).

29. Kumar, R. & Raghavan, S.R. Thermo-thickening in solutions of telechelic associating polymers and cyclodextrins. *Langmuir* in press (2009).

30. Kumar, R., Kalur, G.C., Ziserman, L., Danino, D. & Raghavan, S.R. Wormlike Micelles of a C22-Tailed Zwitterionic Betaine Surfactant: From Viscoelastic Solutions to Elastic Gels. *Langmuir* **23**, 12849-12856 (2007).

Acknowledgements We would like to thank Brian Edwards and Nader Engheta for helpful suggestions and discussion. This work was supported by a DARPA Defense Science Office grant (Grant W31P4Q0910013). E.W. acknowledges funding support from a National Science Foundation CAREER

award (grant number ECCS - 0846494), the Physics Frontier Center at the Joint Quantum Institute, and the Office of Naval Research Applied Electromagnetics Center.

Author contributions C.R, E.W., B. S., and J. T. F. conceived the idea for the paper. Z. C. wrote software for the experiment and C. R. performed the experiments and analyzed the data. S. N. synthesized the nanowires. C.R, E.W., B. S., J. T. F., and S. N. contributed to writing the paper.

Additional Information The authors declare no competing financial interests. Supplementary information accompanies this paper at www.nature.com/naturephotonics. Reprints and permission information is available online at http://www.nature.com/reprints. Correspondence and requests for materials should be addressed to E. W.

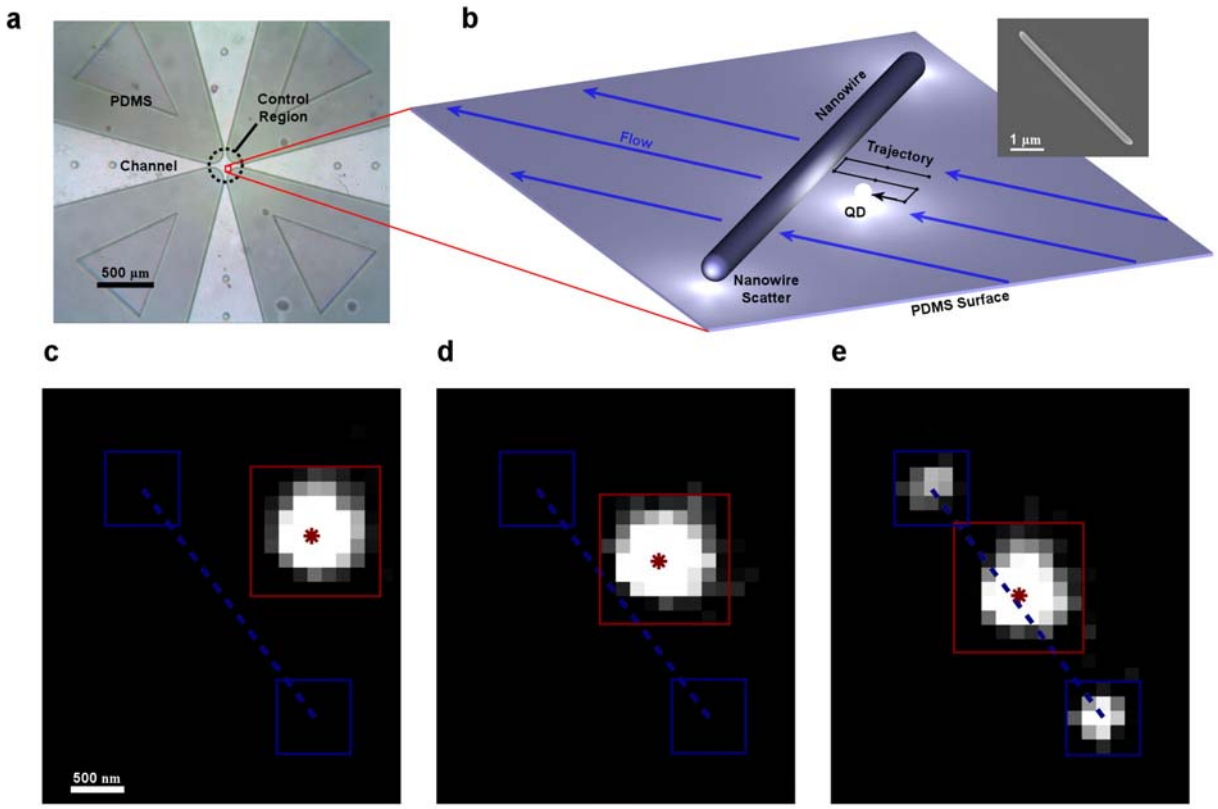

Figure 1 | QD near-field probing. **a.** Optical image of the microfluidic crossed-channel device. Flow in the center control region (dashed circle) is manipulated in two dimensions by 4 external electrodes (not shown). **b.** Illustration of positioning and imaging technique. A single QD is driven along a trajectory close to the wire by flow control and the coupling between the QD and AgNW is measured by the scattered intensity from the wire ends. The inset shows an SEM image of a typical AgNW used in our experiments. **c-e**. A series of emission images showing coupling of the QD to the AgNW as the QD is moved closer to the wire. Intensities are plotted on a log scale. Red (blue) boxes signify the image integration region used to calculate the intensities and positions of the QD (wire scattering points). The measured location of the QD is labeled with a red star and the axis of the AgNW is labeled with a blue dashed line.

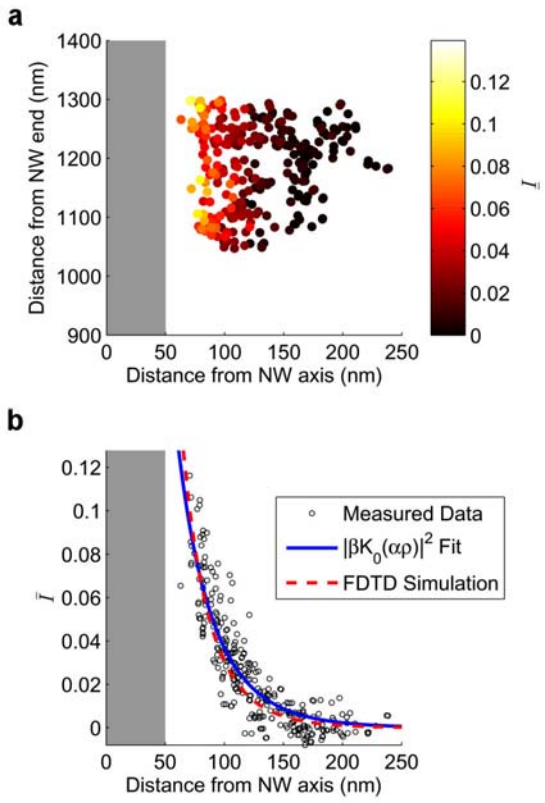

Figure 2 | Probing the evanescent field of an AgNW. a. $\bar{I}$ as a function of position near the middle of the wire. The shaded area indicates the physical extent of the AgNW. **b.** $\bar{I}$ as a function of distance from wire axis using data from panel a. The blue line indicates the best fit to a modified Bessel function. The red line is an FDTD simulation of the AgNW evanescent field. The simulation result was fit to the data using an overall scaling factor.

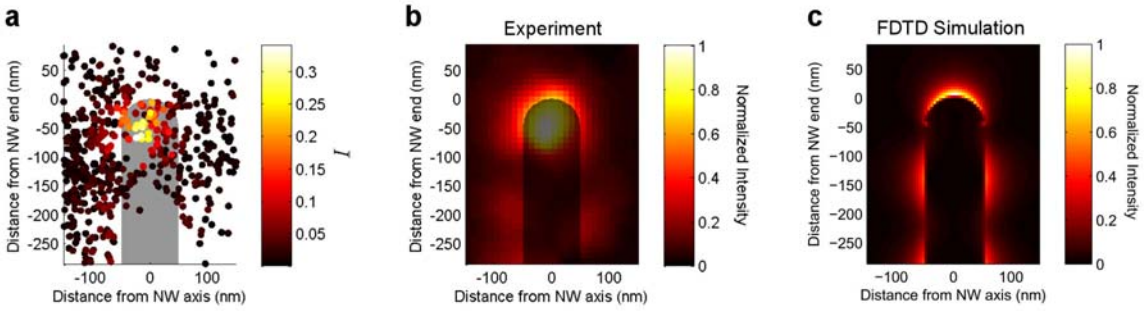

Figure 3 | Evanescent field at the tip of an AgNW. a. Scatter plot of measured positions and intensities near the end of the AgNW. The color of each data point corresponds to $\bar{I}$. The shaded area indicates the position of the wire. **b.** Reconstructed image using a Gaussian weighted average. The image intensity is normalized by its maximum. **c.** FDTD simulation of the AgNW mode profile showing an enhancement at the tip (also normalized by its maximum).

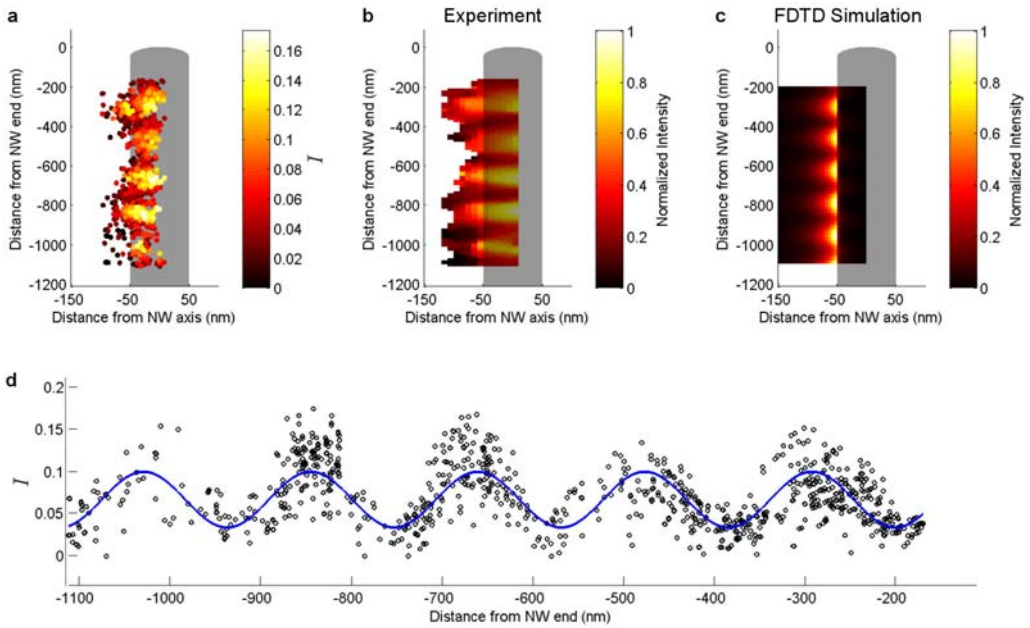

Figure 4 | Probing the mode structure of an AgNW. **a.** Scatter plot of the measured QD positions near the end of the wire. The color of each data point corresponds to $\bar{I}$, measured at each location. The shaded area indicates the position of the AgNW. **b.** Reconstructed image using a Gaussian weighted average. Image intensity is normalized by its maximum. **c.** FDTD simulation of the field intensity standing-wave pattern along the side of the AgNW (also normalized by its maximum). **d.** Circles indicate the measured value $\bar{I}$ as a function of position along the wire. The solid line represents a sinusoidal fit to the data.